Nuclear Engineering and Technology 48 (2016) 952–964

Available online at ScienceDirect

Nuclear Engineering and Technology

journal homepage: www.elsevier.com/locate/net

Original Article

Evaluation of a Sodium–Water Reaction Event Caused by Steam Generator Tubes Break in the Prototype Generation IV Sodium-cooled Fast Reactor

Sang June Ahn[*], *Kwi-Seok Ha*, *Won-Pyo Chang*, *Seok Hun Kang*, *Kwi Lim Lee*, *Chi-Woong Choi*, *Seung Won Lee*, *Jin Yoo*, *Jae-Ho Jeong*, *and Taekyeong Jeong*

Korea Atomic Energy Research Institute (KAERI), 1045 Daedeokdaero, Yuseong, Daejeon 305-353, Republic of Korea

ARTICLE INFO

Article history:
Received 23 May 2015
Received in revised form
3 January 2016
Accepted 10 February 2016
Available online 18 March 2016

Keywords:
Multidimensional Analysis of Reactor Safety-Liquid Metal Reactor
Prototype Generation IV Sodium-Cooled Fast Reactor
Sodium–Water Advanced Analysis Method-II
Sodium–Water Reaction

ABSTRACT

The prototype generation IV sodium-cooled fast reactor (PGSFR) has been developed by the Korea Atomic Energy Research Institute. This reactor uses sodium as a reactor coolant to transfer the core heat energy to the turbine. Sodium has chemical characteristics that allow it to violently react with materials such as a water or steam. When a sodium–water reaction (SWR) occurs due to leakage or breakage of steam generator tubes, high-pressure waves and corrosive reaction products are produced, which threaten the structural integrity of the components of the intermediate heat-transfer system (IHTS) and the safety of the primary heat-transfer system (PHTS). In the PGSFR, SWR events are included in the design-basis event. This event should be analyzed from the viewpoint of the integrities of the IHTS and fuel rods. To evaluate the integrity of the IHTS based on the consequences of the SWR, the behaviors of the generated high-pressure waves are analyzed at the major positions of a failed IHTS loop using a sodium–water advanced analysis method-II code. The integrity of the fuel rods must be consistently maintained below the safety acceptance criteria to avoid the consequences of the SWR. The integrity of the PHTS is evaluated using the multidimensional analysis of reactor safety-liquid metal reactor code to model the whole plant.

Copyright © 2016, Published by Elsevier Korea LLC on behalf of Korean Nuclear Society. This is an open access article under the CC BY-NC-ND license (http://creativecommons.org/licenses/by-nc-nd/4.0/).

* *Corresponding author.*
E-mail address: enginasj@kaeri.re.kr (S.J. Ahn).

http://dx.doi.org/10.1016/j.net.2016.02.016

1738-5733/Copyright © 2016, Published by Elsevier Korea LLC on behalf of Korean Nuclear Society. This is an open access article under the CC BY-NC-ND license (http://creativecommons.org/licenses/by-nc-nd/4.0/).

1. Introduction

The prototype generation IV sodium-cooled fast reactor (PGSFR) has been developed by the Korea Atomic Energy Research Institute. It has a pool-type configuration and uses sodium as a reactor coolant. The reactor is designed to have the capability to produce 150 MWe of electric power. It is composed of primary heat-transfer system (PHTS), intermediate heat-transfer system (IHTS), decay heat removal system (DHRS), and secondary system including the steam generator (SG).

Fig. 1 shows the overall configuration of the PGSFR. The core heat energy is transferred to IHTS sodium through the four intermediate heat exchangers (IHXs) tubes, which are submerged in the cold pool of the reactor vessel. To protect the PHTS in the event of a sodium–water reaction (SWR), the sodium of the closed-loop type IHTS is circulated between the PHTS and SG during normal operation. The high-temperature sodium escaping from the IHX tube is transported to the SG shell, which subsequently transfers its heat to the subcooled water flowing into the SG tubes. Thus, the cooled sodium is eventually transported to the IHX tube by the IHTS pump. The subcooled water supplied by the feed water pump passes through the SG tubes having a vertical single-wall type. It is then transformed into superheated steam by the heat transferred from the hot sodium of the SG shell and is transported to the turbine. The DHRS is operated to remove the residual heat from the core and sensible heat from the PHTS through the four decay heat exchangers (DHXs) submerged in the hot pool of the reactor vessel. It is composed of two loops of passive DHRS (PDHRS) operated with natural circulation flow and two loops of active DHRS (ADHRS) operated with forced circulation flow by an electromagnetic pump. Each train is designed to be capable of removing 50% of the total DHRS heat.

Because of the high pressure difference between the inner and outer parts of the SG tube, a large load is applied to the SG tube surface. The sodium of the SG shell side has chemical characteristics that allow it to react with materials such as water, steam, and oxygen. If an SWR event occurs due to SG tubes leak or break, high-pressure waves and corrosive reaction products are instantaneously generated and propagated to the IHTS components through the IHTS pipes. This event threatens the safety of the reactor and integrity of the IHTS components including the SG tubes. For this reason, an SWR event has been generally considered as one of the design-basis events (DBEs) in sodium-cooled fast reactors.

An SWR is a violent exothermic reaction similar to a simple combustion process [1]. The SWR also generates hydrogen gas that may result in a pressure increase in the system, potentially causing an explosion. Table 1 presents the generally accepted classification of water/steam leaks and dominant damage and threat [2]. The possible causes of an SG tube leak are as follows [3]:

- *Micro leaks (<0.1 g/s):* A micro leak is often developed from an interangular crack in a defected weld and a fatigue crack in a tube wall. The corrosive reaction products often remain in place and plug the leak. The leak may stay plugged for several days or weeks.
- *Small leaks (1–10 g/s):* A small leak often causes localized tube damage, a phenomenon called "self-wastage." The

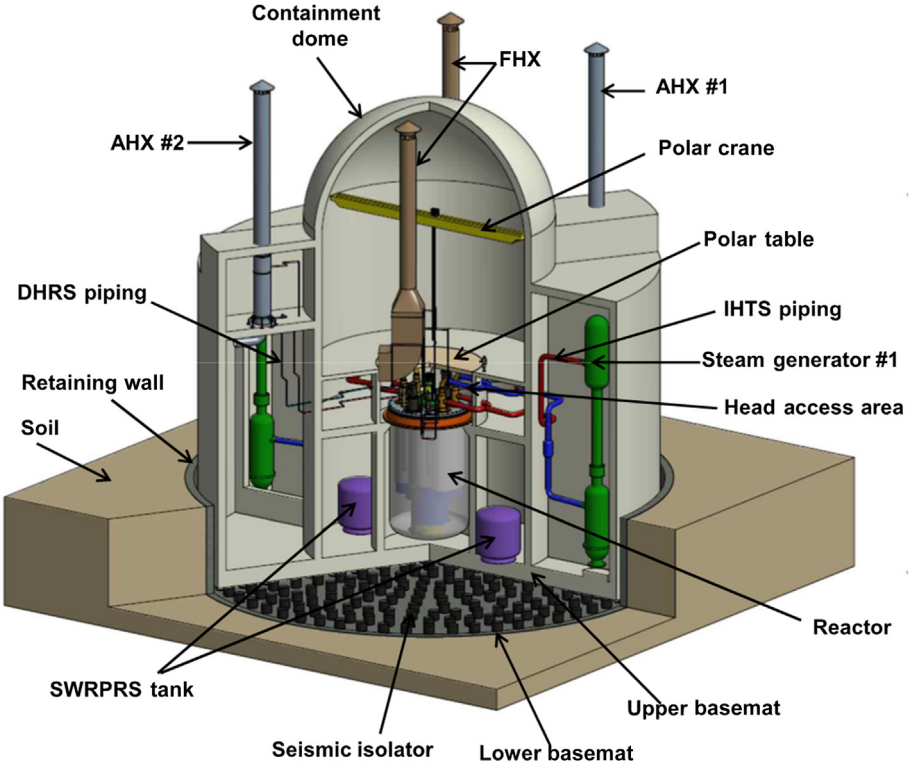

Fig. 1 – Configuration of the prototype generation IV sodium-cooled fast reactor. AHX, natural-draft sodium-to-air heat exchanger; DHRS, decay heat removal system; FHX, forced-draft sodium-to-air heat exchanger; IHTS, intermediate heat-transfer system; SWRPRS, sodium–water reactor pressure relief system.

Table 1 – Classification of water/steam leaks into sodium in a steam generator.

Leak class	Leak rate (g/sec)	Dominant threat
Micro	<0.1	Too small to detect Reaction products form slowly, bubbling may occur No threat to other adjacent tubes
Small	1.0–10	Generate a corrosive sodium–water jet Damage adjacent tubes: Impingement wastage
Intermediate	10–2,000	Lower end: Damage adjacent tubes by wastage Higher end: Tube failure by overheating and pressurization due to hydrogen production (single tube)
Large	>2,000	Rapid pressurization due to hydrogen production (multiple tubes) Tube failure by overheating and overpressure

leak grows by a combination of corrosion and erosion. A small leak can also cause damage to adjacent steam tubes, a phenomenon termed as "impingement wastage." A water jet from a small leak forms a turbulent flow under sodium "flame."

- *Intermediate leaks (10–2,000 g/s):* When the leak rate rises into the intermediate range, the reaction flame becomes large and affects many other tubes. The flame interacts with the flowing sodium and triggers a chaotic turbulent interaction region characterized by widely fluctuating temperatures.
- *Large leaks (>2,000 g/s):* A large leak may cause a rapid increase in pressure in the SG due to a large amount of hydrogen gas generated from SWR. It may cause explosion and damage the components of the secondary cooling circuits.

Based on the classification of the leak rate, two methods to cope with the SWR events are applied to the system design of the PGSFR. For micro-, small-, and intermediate-size leaks, components such as a hydrogen gas detector and acoustic noise sensor are designed to detect the sodium leaks on the surface of SG tubes. For a large-size leak event, a rupture disk as a safety grade and sodium–water reactor pressure relief system (SWRPRS) are designed to mitigate the event and prevent the sequential secondary SWR. In addition, the leak-before-break (LBB) principle is applied to the system design of the pipes and components including the sodium in the PGSFR. The concept of the LBB is applied for large-diameter, high-quality piping systems as a means of enhancing the safety of nuclear power plants [4].

With regard to the PHTS safety, the SWR due to the SG tubes leak or break is categorized as a loss of core cooling capability event. In the PGSFR, the tentatively determined DBEs in relation to the SWR are as follows: (1) events caused by micro or small leaks on the SG tube surface. Here, the "leak rate" is defined as the rate within the range capable of being detected by the sodium leak detection system; (2) events caused by an intermediate or single SG tube double-ended guillotine break (DEGB). Based on the growth and development of leak, the original leak area could be larger, but is not expected to approach that of a double-ended guillotine [5]; (3) events caused by five simultaneous SG tubes DEGB events as large leak DBEs. In the Clinch River Breeder Reactor Project, the DBEs for large leak rate events were defined as a DEGB failure of one SG tube followed by six additional DEGB tube failures with a time lag of 0.1 seconds [6]. In Monju, it is defined as an instantaneous one tube DEGB followed by failure of three tubes as secondary failures [7]. In prototype fast breeder reactors, it is defined as an instantaneous DEGB failure of three tubes at the top of the SG [8].

Based on the process of leak growth and occurrence frequency of the event, simultaneous single or more SG tubes DEGB events have been regarded as being "extremely unlikely." Therefore, the five simultaneous SG tubes DEGB events as large leak DBEs are a very conservative assumption. In addition, because of mitigations such as the operation of the SWRPRS and depressurization in the failed IHTS loop after a rupture disk burst, the consequences following the secondary SWR with a time lag have little influence on the integrity of the IHTS and PHTS.

In the PGSFR, the safety evaluation of the SWR is performed according to the aforementioned classifications. The first evaluation is applied to an event caused by a small leak rate relatively lower than a single SG tube DEGB. If this event occurs, the leaks are detected by the leak detection system and alerted to the operator by an alarm. The operator then manually shuts down the reactor and repairs the failed tubes. A second evaluation is applied to the large leak rate event caused simultaneous one or more SG tubes DEGB. The initial high-pressure waves are propagated to the IHX tube through the IHTS loop pipes in a millisecond order. Upon reaching the burst pressure of a rupture disk, the sodium of the affected IHTS loop is immediately discharged to the sodium dump tank (SDT). Once a rupture disk bursts, the reactor protection system (RPS) signal is produced. To prohibit the subsequent secondary SWR by the continuous release of water or steam through the failed SG tubes, the isolation valves separately connected to the feed water and steam lines of the SG are automatically closed by SWRPRS. For large leak rate SWR DBEs, the structural boundaries of the affected IHTS and SG can be protected from the high-pressure waves produced following a secondary SWR by shutting down the reactor, thereby retaining its integrity.

In this paper, we evaluated the integrity of IHTS and reactor for a large leak rate SWR DBE using the sodium–water advanced analysis method-II (SWAAM-II) code, which is capable of modeling the SWR phenomena, and multidimensional analysis of reactor safety-liquid metal reactor (MARS-LMR), which is capable of modeling the behaviors of the PHTS.

2. Preliminary evaluation of the IHTS integrity

2.1. *Analysis methods and SWAAM-II input modeling*

To evaluate the integrity of the IHTS in the event of a large leak SWR, the SWAAM-II [9] code, which was developed in the Argonne National Laboratory, was used. SWAAM-II is

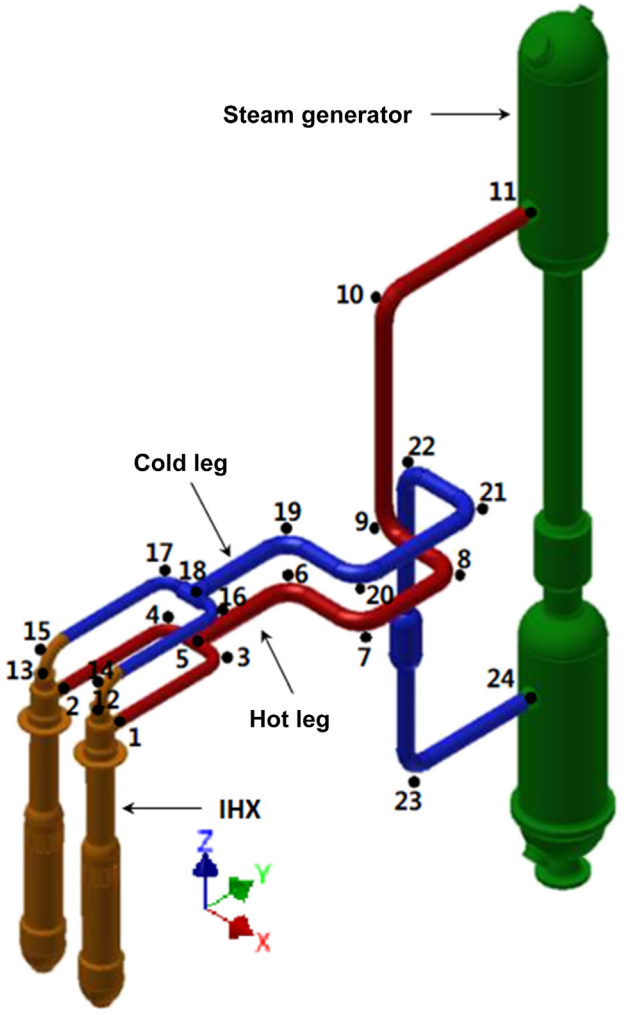

Fig. 2 – One intermediate heat-transfer system loop configuration in the prototype generation IV sodium-cooled fast reactor. IHX, intermediate heat exchanger.

intended to analyze the pressure pulse propagation in a liquid metal fast breeder reactor piping system, which results from an instantaneous failure of the SG tube. It is composed of modules capable of modeling the following phenomena: (1) thermochemical dynamics of the SWR including phase changes of the reaction products; (2) bubble growth of the reaction products; (3) wave propagation and phase changes in the water and steam systems caused by depressurization at the tube break; (4) pressure pulse propagation in the faulted SG; (5) dynamic deformation and failure of the rupture disk systems; (6) dynamic deformation of the SG shell.

The energy equation in the reaction bubble zone can be described through Eq. (1).

$$\frac{d}{dt}\left[\overline{m}u + m'C\left(T - T_{\mathrm{ref}}\right)\approx\right] = \left(\Delta H + \alpha_N h_N + \overline{h}\right)\frac{dm'}{dt} + \overline{h}\frac{d\overline{m}}{dt} - q_f - q_s - pV \tag{1}$$

where $\overline{m}$ is unreacted water mass in the bubble; u is the internal energy of the unreacted water in the bubble; m' is the reacted water mass; C is the total heat capacity of the reaction products; α' is the mass of hydrogen gas generated per unit mass of water reacted; T_{ref} is the reference temperature to measure all energy quantities; ΔH is the heat of reaction; α_N is the mass of sodium per unit mass of water reacted; h_N is the enthalpy of sodium; $\overline{h}$ is the enthalpy of injected water, q_f is the heat loss at the bubble–sodium interface; q_s is the heat loss to solid inclusions such as the tube bundle; p is the bubble pressure; T is the bubble temperature; and V is the bubble volume. The left side of Eq. (1) represents the increase in total bubble energy, and the right side represents the heat source, heat loss and, expansion work.

The expanded form, written as Eq. (2), is more convenient for the purposes of computation.

$$\overline{m}\frac{du}{dt} + Cm'\frac{dT}{dt} = \left[\Delta H + \alpha_N h_N + \overline{h} - C\left(T - T_{\mathrm{ref}}\right)\right]\frac{dm'}{dt} - \left(u - \overline{h}\right)\frac{d\overline{m}}{dt} - q_f - q_s - pV \tag{2}$$

At the reaction bubble and sodium interface, the momentum equation is as follows:

$$P = P_R + \rho\left\{a\left(1 - \frac{a}{R}\right)\frac{d^2a}{dt^2} + \left(\frac{3}{2} - 2\frac{a}{R} + \frac{1}{2}\left(\frac{a}{R}\right)^4\right)\left(\frac{da}{dt}\right)^2\right\} \tag{3}$$

where a is the bubble radius and P_R is pressure at the SG shell radius. This equation is related to the bubble dynamics in the reaction zone.

Because of the instantaneous expansion of a reaction bubble, the generated high-pressure pulses are propagated from the reaction bubble zone to components such as a rupture disk and IHX tube through the IHTS pipes. For large leak SWR DBEs, peak pressures that build up at the components are calculated using SWAAM-II and analyzed.

The SWAAM-II input is based on the predesign data in the PGSFR. Fig. 2 shows the overall configuration of one IHTS loop. It is composed of two IHXs, one hot leg pipe, one cold leg pipe, one expansion tank, and one IHTS pump. In this figure, the red and blue lines represent a hot leg and cold leg with a 0.559 [m]. outer diameter, respectively. The two rupture disks and the corresponding SDT are not shown in this figure.

Fig. 3 shows the nodalization for the SWAAM-II input. A total of 77 pipes and 76 junctions were used for modeling the sodium of the closed-loop type IHTS. As an SWRPRS, one rupture disk with a reverse buckling type and one SDT as a pair are connected with the pipe of the hot leg and cold leg, respectively. An expansion tank filled with argon inert gas is connected with the hot leg to control and maintain the design pressure of the IHTS. The numbers inside the hollowed circle represent the junction number to connect the pipes with each other. The blue and red boxes represent the major interested positions, such as the SG inlet and outlet, expansion tank, IHX inlet, outlet, and IHX active tubes. On the right side of the figure, the vertically arranged pipes and junctions represent the sodium side of the SG shell and the corresponding positions of the SG tube filled with water and steam. The SG tube side is composed of 18 pipes and 19 junctions. As the boundary conditions, pressure and temperature values of 17.2 MPa and 230°C for the inlet and 16.7 MPa and 512°C for the outlet were applied to time-dependent volumes 1 and 2, respectively.

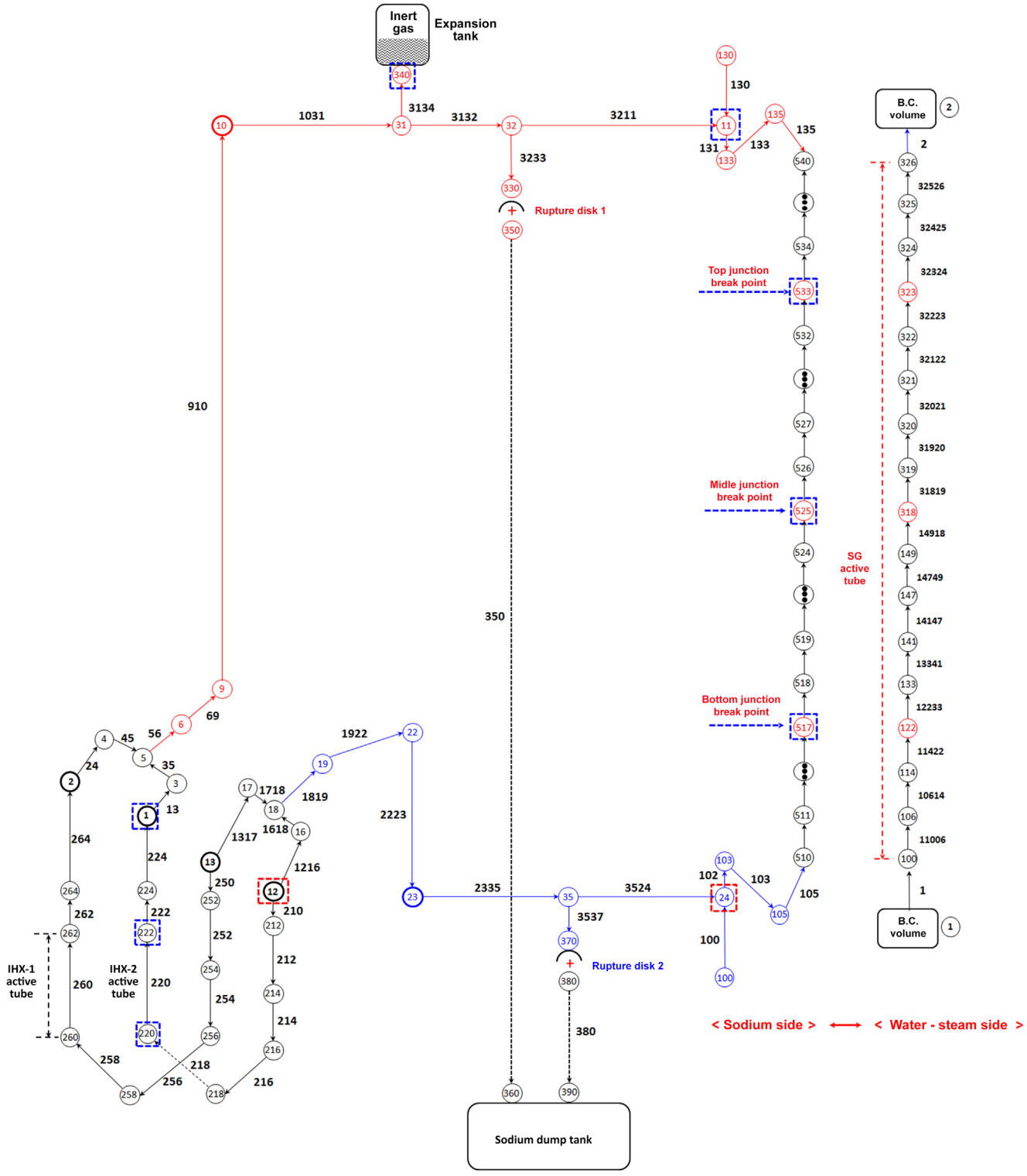

Fig. 3 – Nodalizationfor sodium–water advanced analysis method-II input. B.C., Boundary Condition; IHX, intermediate heat exchanger; SG, steam generator.

2.2. *Evaluation results and discussion*

Prior to calculating large leak SWR DBEs, the peak pressure at the break positions of the SG tube is determined and then analyzed for multiple SG tubes DEGB. The following conditions and assumptions were applied: the burst pressure of the rupture disk is set to 1.0 MPa and a single SG tube DEGB is assumed.

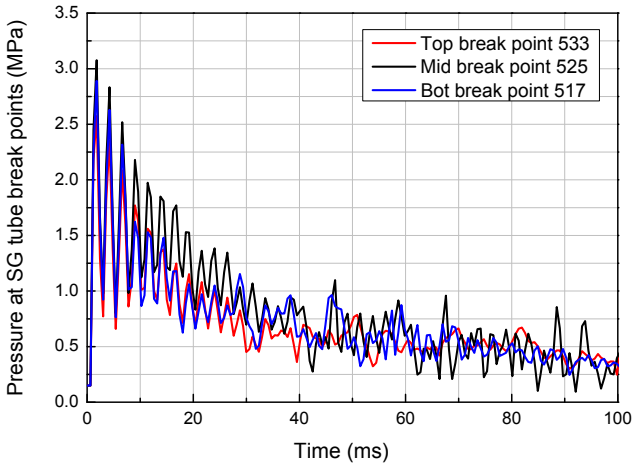

Fig. 4 – Pressures histories at the steam generator tube break points (1 double-ended guillotine break, rupture disk burst pressure = 1.0 MPa). SG, steam generator.

Fig. 4 shows the pressure histories at three break levels of the SG tube. The numbers 533, 525, and 517 are the break locations at the top, middle, and bottom levels of the SG tube, respectively. In the three break positions, the peak pressures were achieved within 5 ms; however, these then gradually decreased due to the cushion effect of the reaction product gas volume. The peak pressure is calculated to be approximately 3.1 MPa at the middle break levels. At the top and bottom break levels, the peak pressures are relatively lower, which is influenced by the configuration of the SG chamber at the top and bottom levels.

Fig. 5 shows the pressure histories at the SG inlet and outlet, respectively. In Fig. 5A, the pressures at the SG inlet are maintained at the initial values before reaching the pressure waves generated from the break positions of the SG tube. Upon reaching the pressure waves, the peak pressures are generated close to the SG inlet and then decreased due to the burst of the rupture disk. The closer the distance between the SG inlet and SG tube break positions, the higher the peak pressure generated. Fig. 5B demonstrates a behavior similar to that witnessed with the SG inlet. Compared with the initial pressures in the SG tube break positions, the propagated pressures to the SG inlet and outlet are significantly decreased to approximately 50%. Because the expansion tank is connected to the hot leg, the propagated pressures to the SG inlet are calculated a little lower than those of the SG outlet.

Fig. 6 shows the propagated pressure histories at the expansion tank connected to the hot leg. The pressure damping effect by the inert gas is equally applied to the three break cases. From the calculation results of Fig. 5A, the pressure at the expansion tank is generated in propagated order and proportional to the magnitude of the propagated pressure. The higher the pressures that are propagated, the higher the pressures that are built at the expansion tank.

Fig. 7 shows the pressure histories at the IHX inlet and outlet, respectively. In Fig. 7A, the pressures are generated in propagated order after about 30 ms; however, the pressures decrease

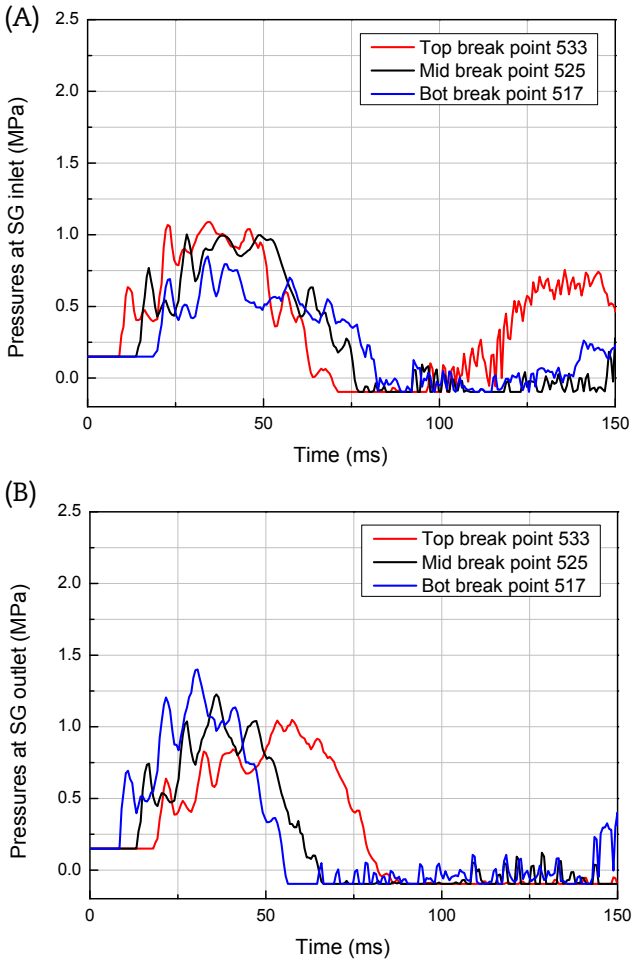

Fig. 5 – Pressures histories at the steam generator (SG). (A) Inlet (J11), (B) outlet (J24; 1 double-ended guillotine break, rupture disk burst pressure = 1.0 MPa).

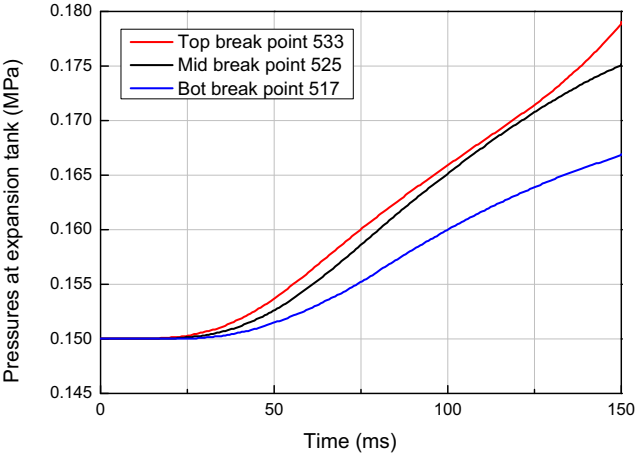

Fig. 6 – Pressure histories at the expansion tank (1 double-ended guillotine break, rupture disk burst pressure = 1.0 MPa).

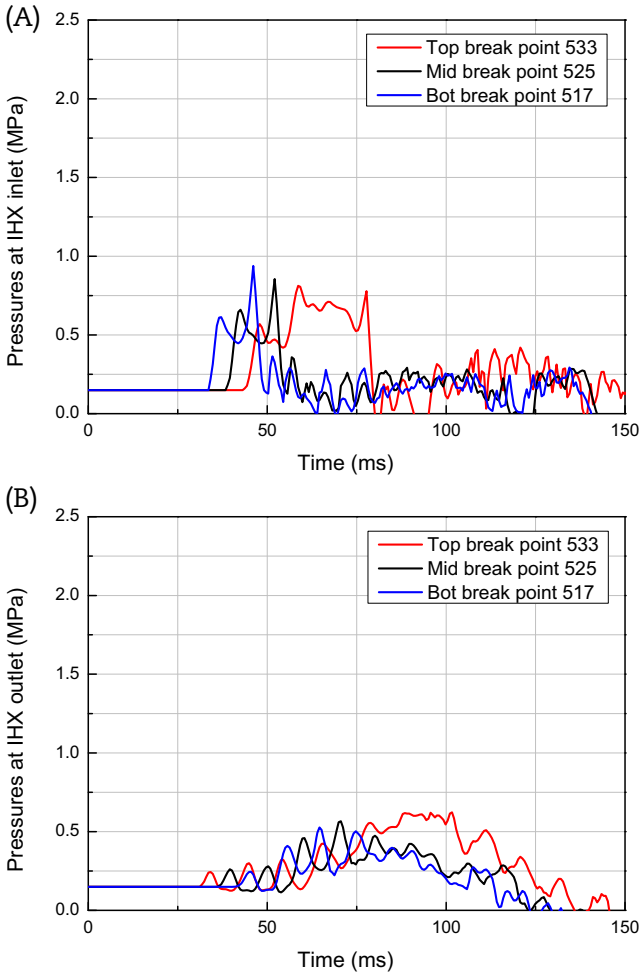

Fig. 7 – Pressure histories at the intermediate heat exchanger (IHX). (A) Inlet (J12) and (B) outlet (J1) (1 double-ended guillotine break, rupture disk burst pressure = 1.0 MPa).

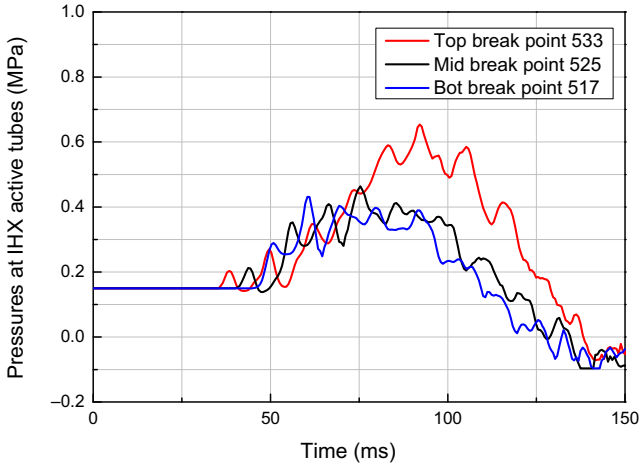

Fig. 8 – Pressures histories at the intermediate heat exchanger (IHX) active tubes (1 double-ended guillotine break, rupture disk burst pressure = 1.0 MPa).

rapidly due to the burst of the rupture disk. In Fig. 7B, the pressure histories show a similar behavior with those of the IHX inlet. Because of the pressure damping effect by the expansion tank, the peak pressures at the IHX outlet are calculated to be relatively lower than the values at the IHX inlet.

Fig. 8 shows the pressure histories at the IHX active tubes, which are an important barrier in terms of radiological defense. For a single SG tube DEGB, the peak pressure is generated when pressure is propagated from the top break level and is approximately 0.65 MPa as shown Fig. 7B. In Fig. 7A, for the IHX inlet, the pressures propagated from the middle and bottom level breaks rapidly decrease to approximately 0.45 MPa due to the geometrical configuration of the IHX. The sodium inflow through the IHX inlet falls vertically down the IHX, passes through the IHX chamber, and then rises up to the IHX active tubes.

From the calculation results for a single SG tube DEGB, the peak pressure in the SG sodium is generated at the middle level of the SG tube. Based on the results in the prior sections,

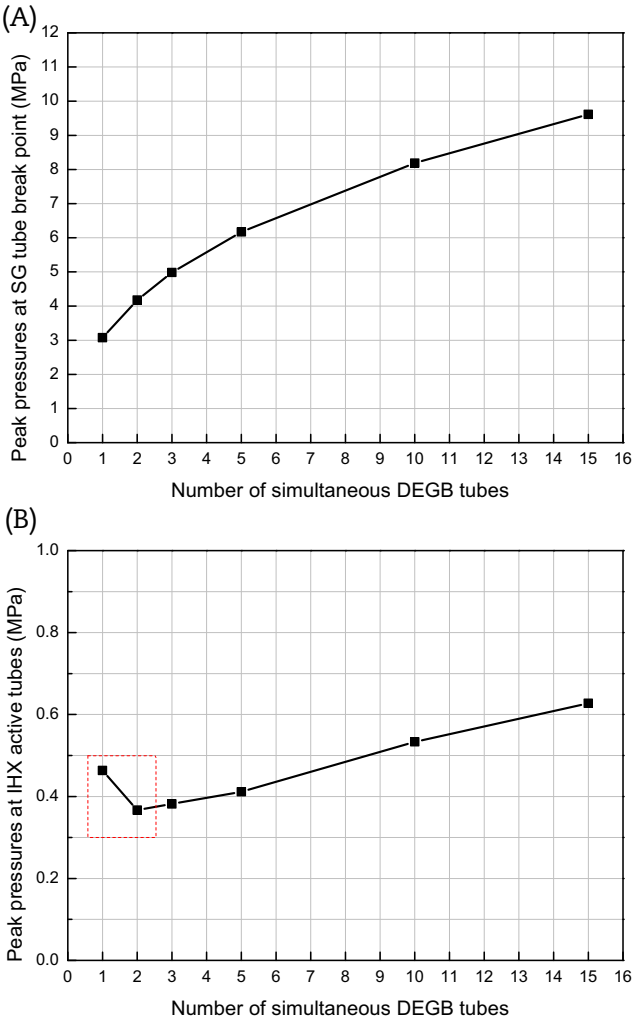

Fig. 9 – Peak pressures. (A) At the steam generator (SG) and (B) at the intermediate heat exchanger active tubes (rupture disk burst pressure = 1.0 MPa). DEGB, double-ended guillotine break.

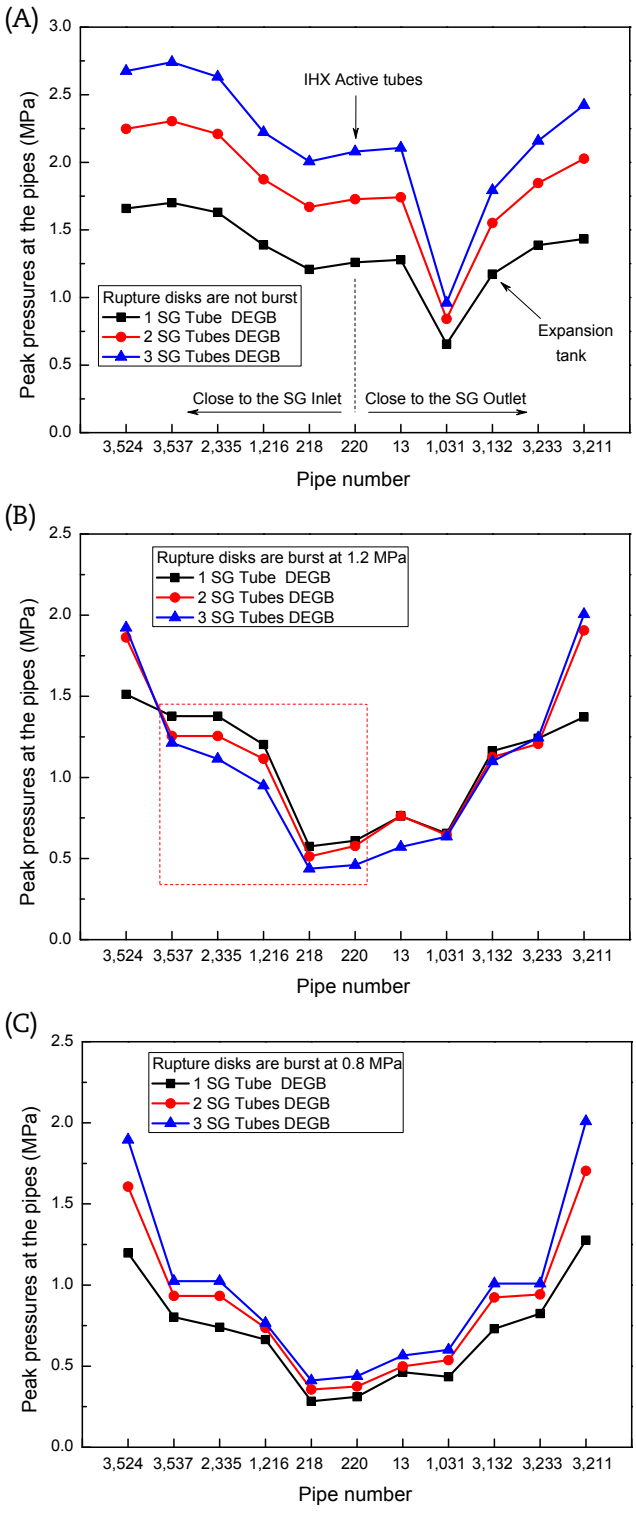

Fig. 10 – Peak pressures at the major pipes of the intermediate heat-transfer system. (A) No burst of the rupture disk, (B) burst pressure of 1.2 MPa, and (C) burst pressure of 0.8 MPa. DEGB, double-ended guillotine break; IHX, intermediate heat exchanger; SG, steam generator.

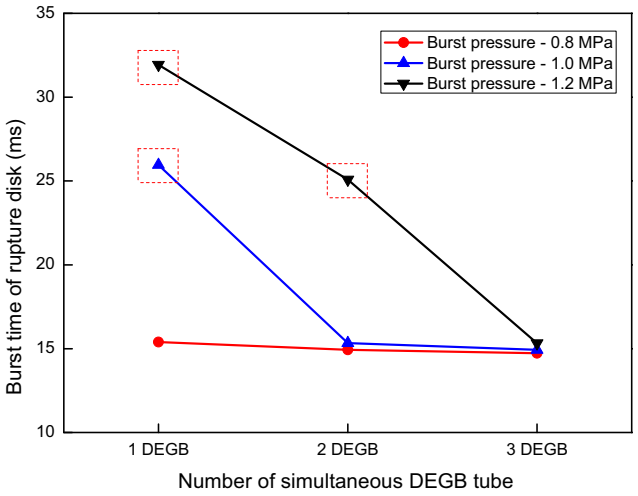

Fig. 11 – Burst time of rupture disk at a burst pressures of the rupture disk. DEGB, double-ended guillotine break.

an evaluation of large SWR DBEs is carried out for events of instantaneous multiple SG tubes DEGB.

Fig. 9 shows the peak pressures at the SG and IHX tubes according to the number of simultaneous SG tubes DEGB. In Fig. 9A, the more the number of simultaneous SG tubes DEGB, the higher linear increase in peak pressures in the SG. In Fig. 9B, the peak pressures in the IHX active tubes are calculated to the unexpected value for a single SG tube DEGB. The analysis for this calculation result is described in Figs. 10 and 11.

Fig. 10 shows the peak pressures at the major pipes of interest according to the burst pressures of the rupture disk and the simultaneous one, two, and three SG tubes DEGB. Fig. 10A shows the peak pressures under the condition of no bursting rupture disks. The pipe numbers are plotted on the x-axis. The pipes to the left of the IHX tube pipe 220 are closer to the SG outlet, whereas those to the right of the IHX tube pipe 220 are closer to the SG inlet. The more the number of the simultaneous tubes DEGB, the higher the peak pressure at the pipes, which is as expected. The peak pressures at pipe number 1031 downstream of the expansion tank are abruptly decreased due to the pressure damping effect at the expansion tank. Fig. 10B shows the peak pressures under the condition of burst pressure of 1.2 MPa of rupture disks. The more the number of the simultaneous tubes DEGB, the lower the peak pressures in the range of pipe numbers 3537 to 220 that are calculated. Fig. 10C shows the peak pressures under the condition of a burst pressure of 0.8 MPa of rupture disks. In the figure, the more the number of simultaneous tubes DEGB, the higher the peak pressures that are calculated, such as the results under the condition of no burst of rupture disks.

Fig. 11 shows the burst time of the rupture disks according to their burst pressures. For a burst pressure of 0.8 MPa (closed circles), the burst times are decreased according to the increase in the number of simultaneous tubes DEGB. For a 1.0-MPa burst pressure (triangles), the burst time for a single tube DEGB is late compared with those of the simultaneous two and three tubes DEGB. For these reasons, the peak pressure at a burst pressure of 1.0 MPa is higher than the peak pressures in the simultaneous two and three tubes DEGB. For a burst pressure of 1.2 MPa (inverted triangles), the burst times are decreased with a significant difference according to the

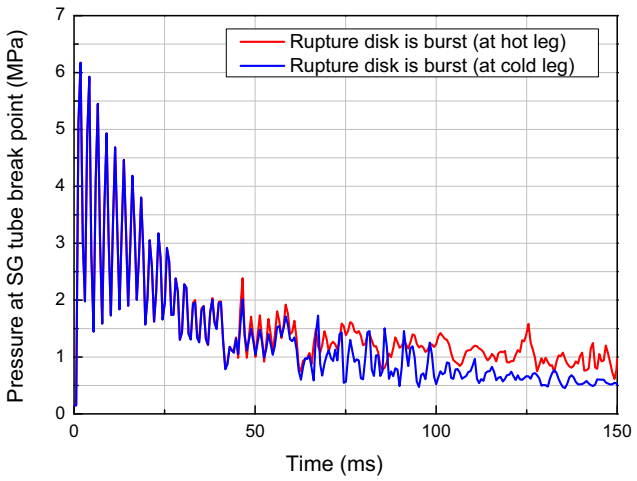

Fig. 12 – Pressures histories at the steam generator (SG) tube break point. Simultaneous five SG tubes double-ended guillotine break, single failure.

increase in the number of simultaneous tubes DEGB. Although the initially generated pressures in the SG can be large according to the increase in the number of simultaneous tubes DEGB, the pressure waves that propagated to the IHX tube can be lower due to the burst time of the rupture disks. Consequently, the faster the burst of the rupture disks, the lower the peak pressure that can propagate to the IHX tube due to depressurization in the affected IHTS loop after the burst of the rupture disks.

Based on the results in the prior section, an evaluation of five simultaneous tubes DEGB for a large leak SWR is carried out. In addition, the single-failure criteria are applied to the rupture disks as a safety measure. Based on these criteria it assumed that one out of two rupture disks failed in the calculation.

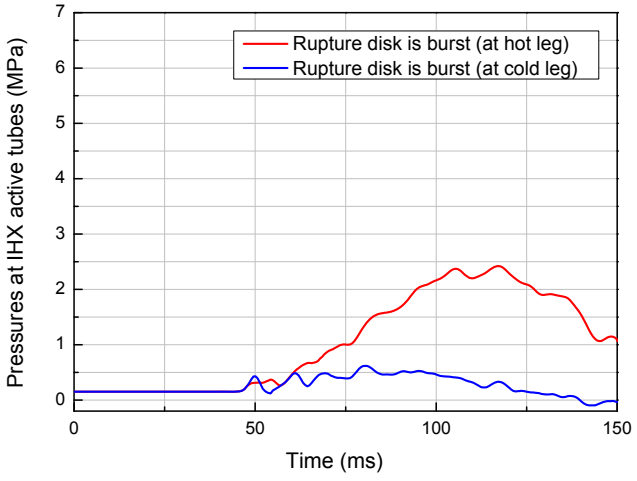

Fig. 13 – Pressures histories at the intermediate heat exchanger (IHX) active tubes. Simultaneous five steam generator tubes double-ended guillotine break, single failure.

Fig. 12 shows the pressure histories calculated at the middle break level of the SG tube. In the figure, the red curve means that the single failure criteria are applied to the rupture disk connected with the cold leg. Thus, during the calculation time, the rupture disk connected with the hot leg normally bursts, but the rupture disk connected with the cold leg is assumed to have failed. In addition, the blue curve is a result of applying a reverse assumption. From the results of the two cases, the build peak pressures are calculated to equal values of approximately 6.2 MPa regardless of the connected position of the rupture disks. Because of the cushion effects of the reaction product gas volume and the burst of the rupture disk, the initial peak pressures are gradually decreased as time passes. Based on the installed level of the rupture disks, the level of the rupture disk connected with hot leg is higher than the level of the rupture disk connected with the cold leg. For this reason, in the case of a burst of the rupture disk connected with the hot leg, the initially generated pressure waves remained at a high state in the SG.

Fig. 13 shows the pressure histories at the IHX inlet and outlet. As shown in the figure, before reaching the pressure waves propagated from the SG, the initial pressures are constantly maintained until approximately 40 ms. As described in Fig. 12, the peak pressure in the case of burst of a rupture disk connected with the hot leg is built higher than that of the cold leg due to the installed level of the rupture disk. For five simultaneous SG tubes DEGB, the peak pressure of the IHX tube is calculated as approximately 2.5 MPa.

3. Transient analysis for SWR

3.1. *Analysis methods and MARS-LMR input modeling*

If an SWR occurs, the integrity of the reactor vessel must be retained and the fuel rods should satisfy the safety acceptance criteria. In the PGSFR, general transients are analyzed using the MARS-LMR [10]. A liquid metal coolant property table, wall heat-transfer coefficients, and the friction factor correlations related to a liquid metal reactor system were added to the MARS code [11] to be used in an analysis of the transients for a liquid metal-cooled reactor system.

As described in the prior section, the reactor is not scrammed until the rupture disk in the SWRPRS bursts because the RPS signal is coupled with the burst of the rupture disk. For a conservative calculation, the transient calculation is initiated under the assumption that the sodium inventory of a failed IHTS loop is fully drained into the SDT. The mass flow rate is set to zero for modeling the sodium of the affected IHTS loop.

A few conservative assumptions such as a loss of offsite power (LOOP) and single failure criteria for DHRS are applied to the transient calculation. For DHRS, one ADHRS train is failed by the assumption of the single failure criteria and one PDHRS train is failed for the maintenance. The event scenario for a transient calculation is as follows: (1) In 5 seconds, the mass flow rate of the failed IHTS loop sodium is decreased to zero. In an actual scenario, however, the amount of sodium drained in the SDT can be restricted by the geometrical arrangement of the IHTS, and drain time can be longer than 5

Table 2 – Event scenario for sodium–water reaction.

	Event scenario	Time (sec)
1	Initial condition for event: Because of steam generator (SG) tubes double-ended guillotine break, the sodium–water reaction event occurs in the SG. The sodium in the one failed intermediate heat-transfer system (IHTS) loop is totally drained. (mass flow rate at flow BC = 0.0 kg/sec)	5
2	Reactor trip signal is initiated	5
3	Reactor + loss of offsite power (2 reactor coolant pumps, 1 IHTS pump, and 1 feed water pump are stopped)	10
4	Air dampers are fully opened (at the natural-draft sodium-to-air heat exchanger/forced-draft sodium-to-air heat exchanger)	15
5	Maximum temperature in the fuel rods: 881.8 K (608.7°C)	120

seconds; (2) a reactor trip signal occurs at 5 seconds; (3) considering the reactor trip signal delay time and LOOP assumption, reactor, reactor coolant pump (RCP), IHTS pump, and feed water pump are simultaneously stopped at 10 seconds. Compared with a light water reactor, the 5-second reactor trip signal delay time is a conservative assumption with respect to the PHTS cooling; and (4) air dampers in the DHRS are fully opened at 15 seconds. In addition, 10 seconds applied to open air dampers of the DHRS to remove the decay heat from the core is a conservative assumption. Table 2 shows a brief event scenario during the transient calculation.

Fig. 14 shows the nodalization for the PHTS and a scheme for modeling the failed IHTS loop. In Fig. 14A, the PHTS is composed of a hot pool and cold pool. The four IHXs are used to transfer the heat generated from the core to the IHTS, and the heat structures for the IHX tubes are modeled. The volume of the IHX shell is composed of 24 nodes and connected with Node 105 for modeling the lower cold pool. The upper cold pool is modeled as Node 100 and the upper volume of this node is filled with an inert cover gas. The two RCPs (Node 115 and 145) connected with the Node 105 are supplied with sodium coolant of the cold pool to the inlet plenum (Node 168) of the core. The inflow sodium to the inlet plenum is heated upon passing through the core (Nodes 175, 178, 180, and 190) and transferred to the core outlet (Node 200). Considering the single failure criteria of the one train ADHRS and the maintenance of the one train PDHRS, the DHRS is modeled as one train ADHRS and one train PDHRS. The DHRS is composed of the two DHX nodes (Nodes 242 and 252), which are submerged into the cold pool, loop pipes, the natural-draft sodium-to-air heat exchanger (AHX; Node 815), and the forced-draft sodium-to-air heat exchanger (FHX; Node 915) to exchange heat with the air.

Fig. 14B shows the scheme of one failed IHTS loop for modeling the SWR with MARS-LMR. To simulate the behavior of the failed IHTS under normal operation conditions, two time-dependent volumes are applied to the hot leg and cold leg, respectively. As a pressure boundary condition, 0.536 MPa for the sodium pressure is applied to the time-dependent volume connected with the hot leg. As a flow boundary condition, 378.9 kg/s mass flow rate of sodium is applied to the time-dependent junction prior to connecting the time-dependent volume with the cold leg. When an SWR occurs, the mass flow rate of the cold leg is set to zero to model the sodium inventory dump to the SDT in the failed IHTS loop.

3.2. *Evaluation results and discussion*

Based on the event scenario for a transient calculation, the evaluation of the PHTS and fuel rods for a large leak SWR is carried out. Fig. 15 shows the behaviors in the PHTS during a transient calculation. Fig. 15A shows the mass flow rates in RCPs 1 and 2, which are submerged in the reactor vessel. During the initial 5 seconds, the rated mass flow rate of the RCP in the normal operation is constantly maintained. The transient calculation is initiated at 5 seconds. By the LOOP assumption, the RCPs are simultaneously stopped and the rated mass flow rates start to decrease at about 10 seconds, considering the reactor trip delay time of 5 seconds. The mass flow rates are gradually decreased by the failure of the RCPs power during approximately 15 seconds, and the natural circulation flow is then built and maintained. Fig. 15B shows the behavior of the reactor power during the transient calculation. During the initial 5 seconds, the rated power of 392.2 MWt is constantly maintained. Considering the LOOP assumption and reactor trip signal delay time, the reactor is stopped due to the shutdown control rod insertion for scramming the reactor at 10 seconds, and the reactor power is then rapidly decreased in a few seconds. After this time, the decay heat power [12] generated from the core is gradually decreased over time.

Fig. 16 shows the heat-transfer rates in the four IHXs and one intact SG. In Fig. 16A, the heat-transfer rates of 100.58 MW of IHX 1 and 2 in relation to the failed IHTS loop are decreased by the flow boundary condition for the mass flow rates at 5 seconds, and these then reach zero at approximately 20 seconds. Because of the LOOP assumption, the heat-transfer rates of the intact IHX 3 and 4 start to decrease at 10 seconds and then maintained by a natural circulation flow after 30 seconds. The heat-transfer rate of 201.58 MW of the intact SG shows an equal behavior with the intact IHX 3 and 4. Fig. 16B shows the heat-transfer rates in the AHX and FHX during a transient calculation. Under normal operation conditions, the sodium of the PDHRC and ADHRC are circulated to prevent solidification and to remove the specified heat in the PHTS. For this reason, the initial heat-transfer rates are constantly maintained until 15 seconds. After 15 seconds, the heat-transfer rates are increased by opening the air dampers by the actuation of the decay heat removal signal. At the initial time, the heat-transfer rates of the shell side in the AHX and FHX are significantly increased higher than those on the tube side due to the direct influences by the opening of the air dampers. After 1,000 seconds, the heat-transfer rates of the ADHRS are maintained higher than those of the PDHRS due to the forced circulation flow.

Fig. 17 shows the maximum temperature of the fuel rods during the transient calculation. Before 10 seconds, the temperature of the fuel rods is maintained at approximately 900.7 K (627.6°C). Upon initiating the shutdown control rod insertion by the RPS trip signal actuation, the temperature of the fuel rods is abruptly decreased to approximately 701.5 K (428.4°C). At the suspension of the two RCPs, one intact IHTS

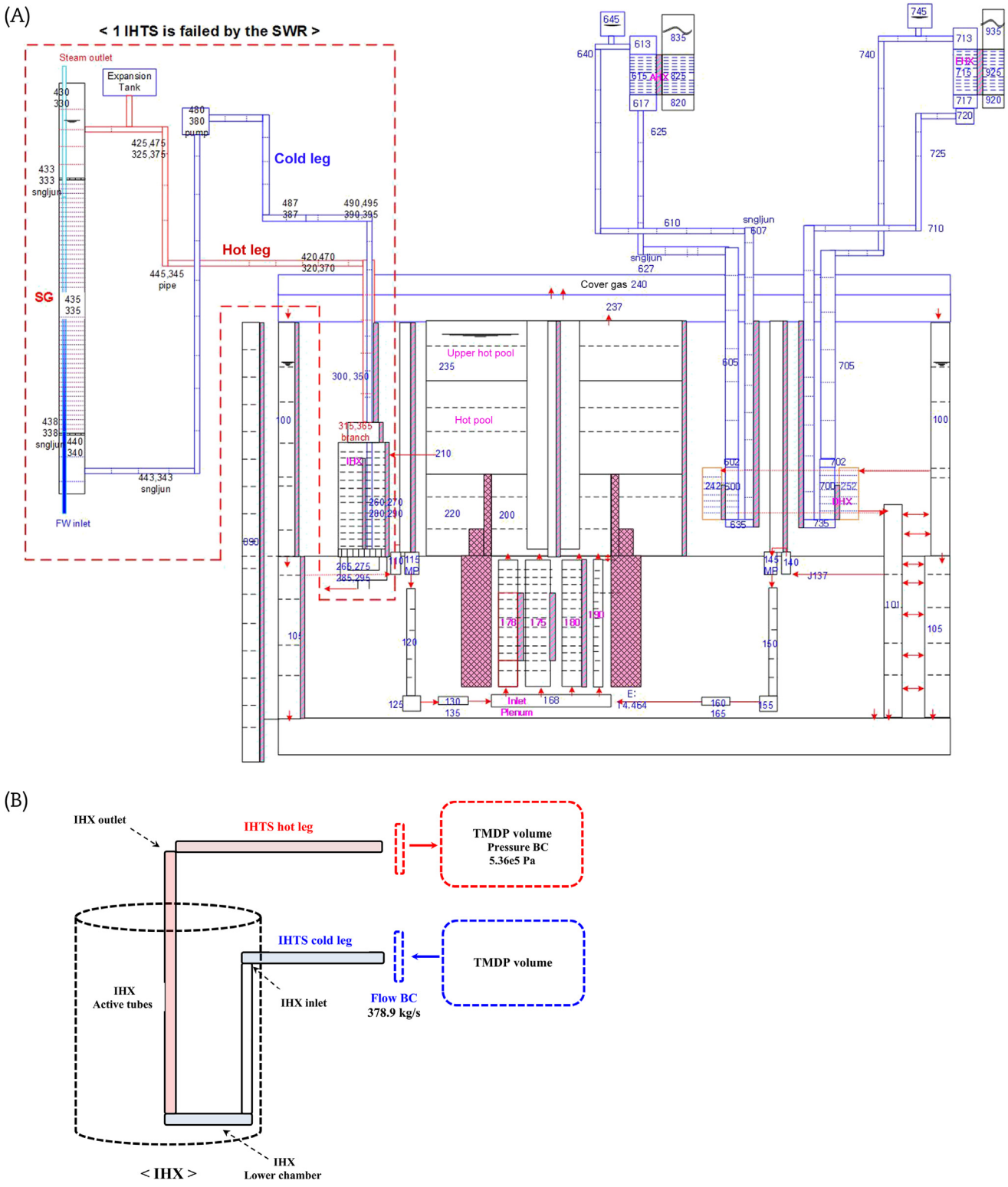

Fig. 14 – (A) Nodalization and (B) scheme for multidimensional analysis of reactor safety-liquid metal reactor input. BC,; IHTS, intermediate heat-transfer system; IHX, intermediate heat exchanger; SG, steam generator; SWR, sodium–water reaction; TMDP.

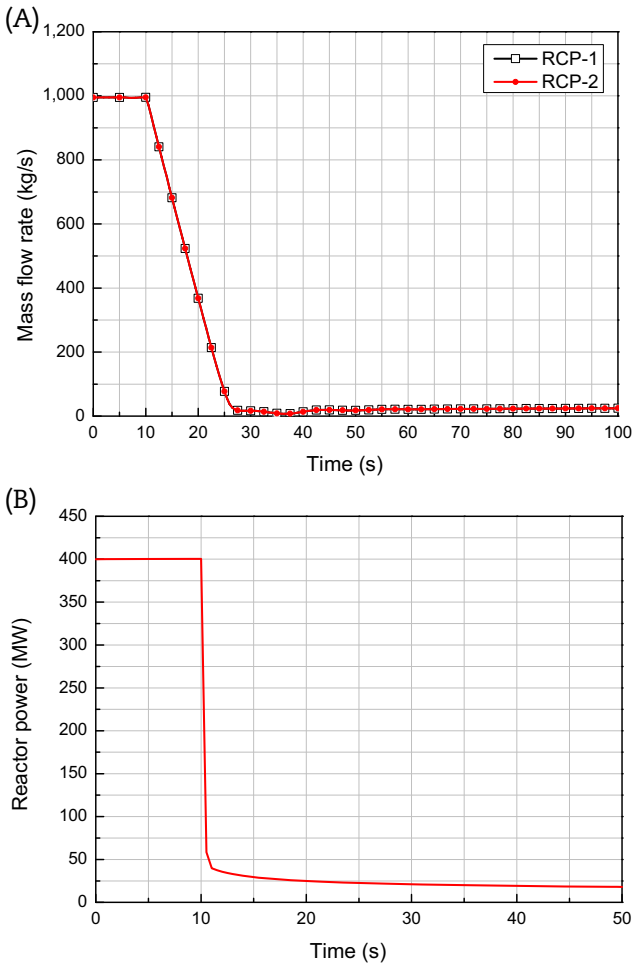

Fig. 15 – Behavior of the reactor coolant pump. (A) Mass flow rate and (B) reactor power during a transient calculation. RCP, reactor coolant pump.

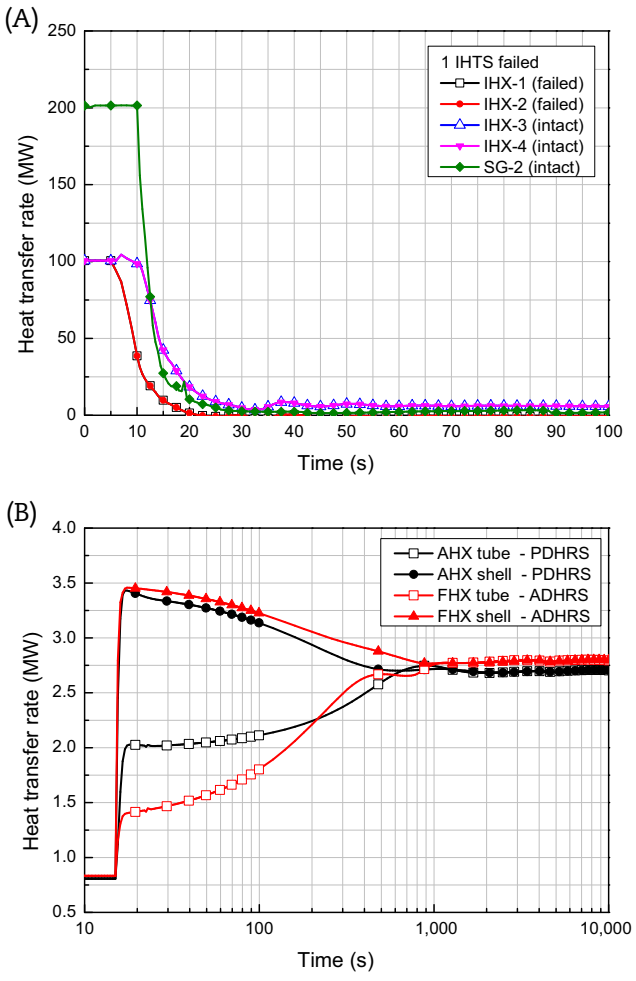

Fig. 16 – Heat-transfer rates. (A) Of the intermediate heat exchanger and (B) of the decay heat removal system during a transient calculation. ADHRS, active decay heat removal system; AHX, natural-draft sodium-to-air heat exchanger; FHX, forced-draft sodium-to-air heat exchanger; IHTS, intermediate heat-transfer system; IHX, intermediate heat exchanger; PDHRS, passive decay heat removal system; SG, steam generator.

pump and one feed water pump by the LOOP assumption, the temperature increases due to the decay heat from the core and the sensible heat in the PHTS. The maximum temperature of the fuel rods is calculated as approximately up to 881.8 K (608.7°C) at 120 seconds. After 100 seconds, the temperature of the fuel rods is gradually decreased by the operation of the DHRS after 15 seconds. For the one IHTS loop failure event due to a large leak SWR, the maximum temperature of the fuel rods is well within the normal operating temperature range for the fuel rods and core.

3.3. *Conclusions*

For sodium water reaction events by the leak or break of SG tubes, the evaluation of the integrity of the IHTS and PHTS is performed using the SWAAM-II and MARS-LMR codes in the PGSFR.

Based on the calculation results obtained using SWAAM-II, the peak pressure in the SG is generated at the middle level of the SG tube. Because of the pressure damping effect in the expansion tank, the pressure waves propagated to the hot leg direction are calculated lower than those toward the cold leg

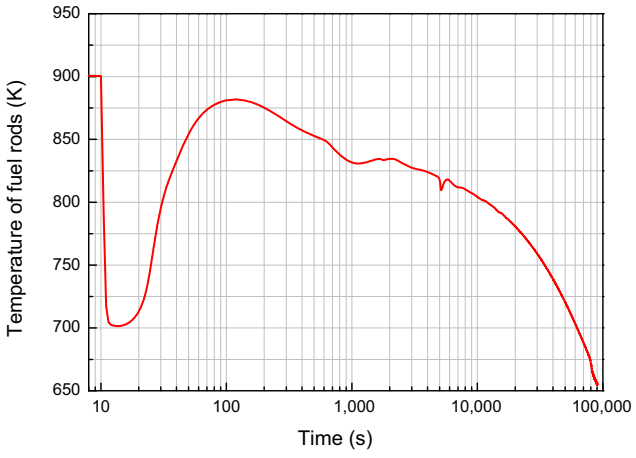

Fig. 17 – Temperature of the fuel rods during a transient calculation.

direction. For a single SG tube DEGB, the generated peak pressure of the SG and IHX tube are calculated to be approximately 3.1 MPa and 0.65 MPa, respectively. For a five SG tubes DEGB, the peak pressures in the SG and IHX tube are calculated as 6.2 MPa and 2.5 MPa, respectively.

In the evaluation of the integrity of the PHTS through the MARS-LMR, the maximum temperature of the fuel rods is calculated as approximately 881.8 K (608.7°C) at 120 seconds. Although conservative assumptions such as the reactor trip delay time, LOOP assumption, and single failure criteria are applied to the event scenario, the integrity of the fuel rod is well within the normal operating temperature range for one IHTS failure event due to the five simultaneous SG tubes break.

Conflicts of interest

All authors have no conflicts of interest to declare.

Acknowledgments

This work was supported by the National Research Foundation of Korea (NRF) grant funded by the Korean government MSIP (No. 2012M2A8A2025634).

Nomenclature

C	total heat capacity of the reaction products;
$\overline{h}$	enthalpy of injected water;
h_N	enthalpy of sodium;
$\overline{m}$	unreacted water mass in the bubble;
m'	reacted water mass;
p	bubble pressure;
q_f	heat loss at the bubble–sodium interface;
q_s	heat loss to solid inclusions such as the tube bundle;
T	bubble temperature;
T_{ref}	reference temperature to measure all energy quantities;
u	internal energy of unreacted water in the bubble;
V	bubble volume;
α'	mass of hydrogen gas generated per unit mass of water reacted;
α_N	mass of sodium per unit mass of water reacted; and
ΔH	heat of reaction.

REFERENCES

[1] D.A. Greene, Sodium-water reaction phenomena associated with small leaks in LMFBR steam generator, in: Proceedings of the Third International Conference, Oxford, Vol. 1, 1984, pp. 13–21.
[2] International Atomic Energy Agency, Liquid Metal Cooled Reactors: Experience in Design and Operation (Rep. No. IAEA-TECDOC-1569), International Atomic Energy Agency, Wien (Austria), 2007.
[3] H.-T. Chien, S. Bakhtiari, S.-H. Sheen, Interim Progress Report: Steam Generator Leak Detection System (Rep. No. ANL-KAERI-SFR-13-26), Argonne National Laboratory, Chicago, 2013.
[4] P.M. Scott, R.J. Olson, G.M. Wilkowski, Development of Technical Basis for Leak-Before-Break Evaluation Procedures (Rep. No. NUREG/CR-6765), U.S. Nuclear Regulatory Commission, Rockville (MD), 2002.
[5] Clinch River Breeder Reactor Project, Large Sodium-Water Reaction: Preliminary Safety Analysis Report, U.S., 1975 (Chapter 15.3–46)
[6] D.A. Greene, D.W. Sandusky, Results of small leak behavior and damage propagation tests in the U.S, in: Presented at the 2nd Joint US/USSR Seminar on the Development of Sodium-Cooled Fast Breeder Steam Generators, USSR, July 26, 1976.
[7] E. Wachi, T. Inoue, Detection system of SG tube failure in Monju to limit failure within design basis leak, Presented at IAEA/IWGFR Specialist' Meeting on "Steam Generator: Failure and Failure Propagation," Aix-en-Provence, France, September 26–28, 1990.
[8] P. Chellapandi, Studies towards safety related to sodium in India, Presented at 2nd joint GIF-IAEA/INPRO Consultancy Meeting on Safety Aspects of SFRs, India Gandhi Centre for Atomic Research, India, 2011.
[9] Y.W. Shin, C.K. Youngdahl, User Manual for the Sodium-Water Reaction Analysis Computer Code SWAAM-II (Rep. No. ANL-83-75), Argonne National Laboratory, Chicag, 1975.
[10] K.-S. Ha, H.-Y. Jeong, Comparison of the decay heat removal systems in the KALIMER-600 and DSFR, Nucl. Eng. Technol. 44 (2012) 535–542.
[11] J.J. Jeong, K.-S. Ha, B.D. Chung, W.J. Lee, Development of multi-dimensional thermal-hydraulic system code, MARS 1.3.1, Ann. Nucl. Energy 26 (1999) 1611–1642.
[12] American National Standards Institute (ANSI), American National Standard for Decay Heat Power in Light Water Reactors, ANSI, Washington DC, WA, 1979. ANSI/ANS 5.1.